

Article

Performance of Hybrid Single Well Enhanced Geothermal System and Solar Energy for Buildings Heating

Yujiang He ^{1,2} and Xianbiao Bu ^{3,*}

¹ Institute of Hydrogeology and Environmental Geology, Chinese Academy of Geological Sciences, Shijiazhuang 050061, China; hyj8620@163.com

² Technology Innovation Center of Geothermal & Hot Dry Rock Exploration and Development, Ministry of Natural Resources, Shijiazhuang 050061, China

³ Guangzhou Institute of Energy Conversion, Chinese Academy of Sciences, Guangzhou 510640, China

* Correspondence: buxb@ms.giec.ac.cn

Received: 10 April 2020; Accepted: 13 May 2020; Published: 14 May 2020



Abstract: The energy reserves in hot dry rock and hydrothermal systems are abundant in China, however, the developed resources are far below the potential estimates due to immature technology of enhanced geothermal system (EGS) and scattered resources of hydrothermal systems. To circumvent these problems and reduce the thermal resistance of rocks, here a shallow depth enhanced geothermal system (SDEGS) is proposed, which can be implemented by fracturing the hydrothermal system. We find that, the service life for SDEGS is 14 years with heat output of 4521.1 kW. To extend service life, the hybrid SDEGS and solar energy heating system is proposed with 10,000 m² solar collectors installed to store heat into geothermal reservoir. The service life of the hybrid heating system is 35 years with geothermal heat output of 4653.78 kW. The novelty of the present work is that the hybrid heating system can solve the unstable and discontinuous problems of solar energy without building additional back-up sources or seasonal storage equipment, and the geothermal thermal output can be adjusted easily to meet the demand of building thermal loads varying with outside temperature.

Keywords: single well enhanced geothermal system; shallow depth enhanced geothermal system; deep borehole heat exchanger; hybrid geothermal and solar energy; geothermal heating

1. Introduction

By the end of 2016 in north China, a total of 20.6 billion m² building floor areas had space heating, about 83% of space heating areas used coal boiler or coal CHP (combined heat and power), and the annual coal consumption was 400 million ton-coal-equivalent [1]. A coal based heating system contributes significantly to winter air pollution [2,3]. There is thus an urgent need for clean energy building heating technology at the present stage. Geothermal energy has showed significant potential as a renewable energy resource because of its low environmental impact, low greenhouse gas emissions and its feasible technology [4–6].

The energy reserves in hot dry rock (HDR) within subsurface of 3–10 km depths are more than 2.52×10^{25} J in China [1,4]. To extract heat from HDR, the enhanced geothermal system (EGS) is proposed by creating artificial fractures in the hot rocks and injecting fluid into them [7–10]. At the present stage, the exploiting technology of EGS is immature. Generally speaking, exploiting an EGS is a huge capital investment. Moreover, the creation of the artificial fractures especially in the hard rock has a high risk and a high cost [11–14]. Hydrothermal resources in China are equivalent to 1.25×10^3 billion tons of standard coal, and its recoverable resources per year are equivalent to 1.9 billion tons of standard coal. However, the hydrothermal heating area in China was only 102 million m² by the end of

2015 [1,3]. One of the main causes for the large mismatch between potential estimates and developed hydrothermal resources is the lack of large and continuous geothermal reservoirs.

There are often lots of hydrothermal systems with a single well output of less than $30 \text{ m}^3/\text{h}$ or even less due to low permeability, which leads to the poor economization of exploitation and utilization. One of the alternatives to utilizing low output geothermal wells is the technology of the deep borehole heat exchanger (DBHE), as shown in Figure 1. Some researchers have focused on the utilization of geothermal energy from DBHE for building heating [15–20]. Bu et al. carried out experimental and simulation studies on DBHE for building heating, and concluded that the heat extraction from DBHE can hardly be further improved due to poor thermal conductivity of rocks [21,22]. To enhance the heat transfer between fluid and rocks, the artificial fractures are created in EGS by the technology of hydraulic fracturing in order to form the convection heat transfer. Based on this thought, if the shallow depth hydrothermal system with low permeability and low output can implement hydraulic fracturing like with EGS for building heating, this not only has a good use of structural fissures in hydrothermal system but also reduces the risk and investment costs of EGS. The shallow depth hydrothermal system has natural fractures interconnecting an injection well to a production well, and it is thus easy to conduct hydraulic fracturing and stimulation to create new fractures and highly conductive zones. In this study, a shallow depth enhanced geothermal system (SDEGS) is proposed, which is reformed from the hydrothermal system. The common problems in SDEGS and conventional EGS are basically the same, such as (1) the thermal breakthrough; (2) the risk of induced seismicity; (3) the detection of formation stress distribution; and (4) the control technology of artificial fractures orientation and the isolation technology to reduce the loss of circulating fluid. The achievements from SDEGS are expected to apply to conventional EGS, and thus to accelerate its development.

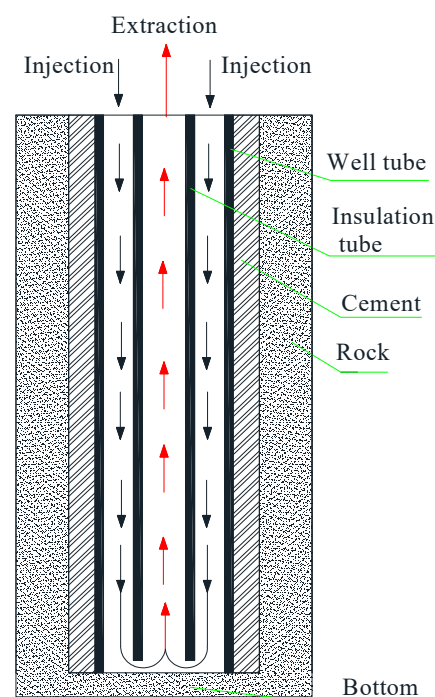


Figure 1. Structure diagram of deep borehole heat exchanger (DBHE).

China has abundant solar energy resources and more than two-thirds of areas receive an annual total solar radiation that exceeds $5.9 \text{ GJ}/\text{m}^2$ with sunshine duration more than 2200 h [23]. However, solar thermal has contributed little for space heating; only about $150,000 \text{ m}^2$ solar collectors were used for space heating in China in 2014 [24]. The above fact is mainly attributed to the unstable and discontinuous energy supply of solar heat, thus back-up sources or seasonal storage equipment are required to ensure the smooth operation of solar space heating system, which leads to high engineering

costs. To circumvent these problems, a hybrid geothermal and solar energy heating system is proposed. Storing heat from solar energy into DBHE is restricted due to rock having poor thermal conductivity. While for SDEGS, the heat convection is formed in the artificial reservoir, whose heat transfer coefficient is far greater than that of heat conduction. If combining SDEGS with solar energy for building heating, solar energy is able to store in geothermal reservoirs during the non-heating season, while during the heating season heat energy is also able to be extracted from geothermal reservoirs. Therefore, a hybrid of SDEGS and solar energy for building heating is recommended in this study. In the hybrid system, the problem of unstable and discontinuous energy supply for solar energy in the heating season can be solved by adjusting geothermal energy output; while in the non-heating season, the heat from solar energy can be stored in geothermal reservoirs to extend the service life of the hybrid heating system. The main aim of this study is to evaluate the performance of the hybrid SDEGS and solar system for building heating.

2. Methods

2.1. System Description

The schematic of SDEGS is illustrated in Figure 2a. The packer is used in order to let circulating fluid flow into an artificial reservoir. In Figure 2a, the depth of the artificial reservoir is 2600 m, with a bottomhole temperature of 87.42 °C and average geothermal gradient of 27.8 °C/km. The diameters for well tube and insulation tube are, respectively, 177.8 and 110 mm. The density, specific heat and thermal conductivity for rocks are respectively 2800 kg/m³, 0.92 kJ/kg/K and 3.49 W/m/K. The artificial reservoir with porosity and permeability of 0.1 and 10^{−12} m² has a thickness of 500 m (from 2100 m to 2600 m) and radius of 50 m. In the hybrid geothermal and solar heating system, the roof-integrated collectors of 10,000 m² are used. The schematic of the hybrid geothermal and solar heating system is shown in Figure 2b. In the heating season, valves 1, 2, 4 and 6 are kept open, and valves 3 and 5 remain closed. SDEGS coupled with heat pump and solar energy systems provide heat for buildings separately, and the supply and return water temperatures of user sides is, respectively, 45 and 40 °C. That is, the inlet and outlet temperature for heat pump and solar system are also, respectively, 45 and 40 °C. In the hybrid system, the heat storage tank provides short-term thermal energy storage on a diurnal basis. If the solar system does not work, the thermal output of the hybrid system can be adjusted by controlling the injection water temperature and volume flow rate of SDEGS in order to meet the need of building heating loads varying with outdoor air temperature. The circulating water with temperature and volume flow rates of, respectively, 5 °C and 50 m³/h is injected into the ring-shaped channel between well tube and insulation tube, and extracted through the insulation tube. In the non-heating season, valves 3 and 5 remain open, and valves 1, 2, 4 and 6 remain closed. The hot water from solar collectors with temperature and daily average volume flow rate of respectively 90 °C and 15.17 m³/h is injected into a geothermal artificial reservoir through the insulation tube, and extracted by the ring-shaped channel. The heating time is 140 days per heating season, and the rest time is used for heat recovery.

In the hybrid geothermal and solar heating system, the evacuated tubular collector is used, and its thermal efficiency is given as follows [25]:

$$\eta = 0.721 - 0.89 \frac{T_m - T_0}{G} - 0.0199 \frac{(T_m - T_0)^2}{G} \quad (1)$$

where, η is thermal efficiency of solar evacuated tubular collector; T_m is average temperature of collector inlet and outlet, °C; T_0 is ambient Temperature, °C; G is direct radiation intensity, W/m². The intensity of solar direct radiation is 600 W/m² for 6 h per day in the heating season in Qingdao, China, and it is 750 W/m² for 7 h per day in the non-heating season.

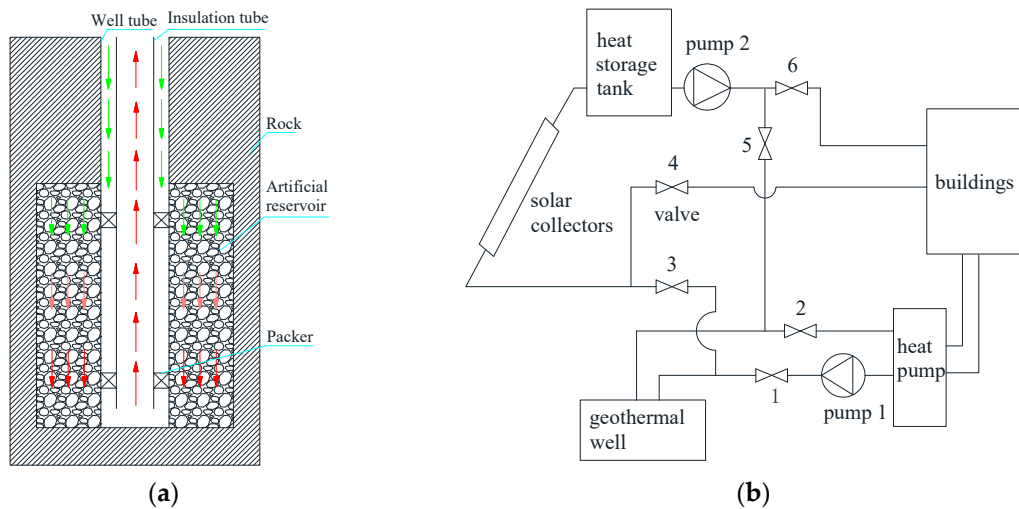


Figure 2. (a) Schematic of shallow depth enhanced geothermal system (SDEGS); (b) schematic of hybrid geothermal and solar heating system.

Facing the engineering application, the following questions related to the hybrid SDEGS and solar energy heating system need to be answered: (1) is the thermal output of the hybrid system stable and sustainable? (2) can the thermal output of the hybrid system be easily adjusted to meet the needs of building heating load variation? These questions are hard to answer by the experimental studies due to the high cost. Alternatively, as a conventional method, numerical simulation can be used to analyze the performance of the hybrid heating system in order to answer the above questions. The mathematical model and its solutions for the hybrid system may refer to the references [26–29].

$$P_t = P_g + P_s \quad (2)$$

where, the symbol P_g represents the thermal output extracted from geothermal artificial reservoir, P_s represents the thermal output from solar collector, P_t is the total thermal output from geothermal and solar energy, and T_{out} is the extracted water temperature from geothermal well.

2.2. Mathematical Model

The assumptions of the mathematical model are listed as follows: (1) the artificial reservoir is assumed to be isotropic and homogeneous and is equivalent to a porous medium having uniform porosity ε and permeability K [30–32]; (2) the flow in artificial reservoir is only the single-phase flow; (3) the rocks enclosing the artificial reservoir are impermeable; (4) the influence of fluid-rock reaction is neglected; (5) the local thermal non-equilibrium between the porous rock matrix and fluid is considered [30–32], and two energy equations are employed.

The governing equations are given as the following.

Fluid continuity equation:

$$\frac{\partial(\varepsilon \rho_f)}{\partial t} + \nabla \cdot (\rho_f \mathbf{u}) = 0 \quad (3)$$

Fluid momentum equation:

$$\frac{\partial(\rho_f \frac{\mathbf{u}}{\varepsilon})}{\partial t} + \nabla \cdot (\rho_f \frac{\mathbf{u}}{\varepsilon} \cdot \frac{\mathbf{u}}{\varepsilon}) = -\nabla P + \nabla \cdot (\mu \nabla \cdot \frac{\mathbf{u}}{\varepsilon}) - \frac{\mu}{K} \mathbf{u} + \rho_f \mathbf{g} \quad (4)$$

Energy equation in the porous rock matrix:

$$\frac{\partial[(1-\varepsilon)\rho c_p T]_s}{\partial t} = \nabla \cdot (\lambda_s^{eff} \nabla T_s) - h_v(T_s - T_f) \quad (5)$$

Energy equation for the fluid:

$$\frac{\partial(\varepsilon \rho c_p T)_f}{\partial t} + \nabla \cdot [(\rho c_p T)_f \mathbf{u}] = \nabla \cdot (\lambda_f^{eff} \nabla T_f) + h_v(T_s - T_f) \quad (6)$$

where, \mathbf{u} , T_s , T_f and P denote the fluid velocity vector, rock matrix temperature, fluid temperature and fluid pressure, respectively; c_p , ρ and λ with subscript “f” and “s” represent specific heat capacity, density and heat conductivity of fluid and rock matrix, respectively. The symbol μ denotes the viscosity of fluid. The heat conductivity of fluid and rock matrix in the artificial reservoir are calculated with the effective forms i.e., $\lambda_s^{eff} = \lambda_s(1 - \varepsilon)^{1.5}$ and $\lambda_f^{eff} = \lambda_f \varepsilon^{1.5}$, where ε is the artificial reservoir porosity [31]. The symbol h_v is the volumetric heat exchange coefficient between fluid and the porous rock matrix.

2.3. Initial and Boundary Conditions

The porosity and permeability of the artificial reservoir are equivalent to 0.1 and 10^{-12} m^2 , respectively [33]. The injection water temperature and volume flow rate are set at 5°C and $50 \text{ m}^3/\text{h}$, respectively. The heating time is 140 days per year in Qingdao, China, and the rest time is used for heat recovery.

The temperatures of rocks keep constant and are not disturbed by the fluid when r is larger than 200 m, as shown in [22,29].

At the interface of artificial reservoir and surrounding rocks, the heat exchange is calculated according to the following formula:

$$h_{sf}(T_s - T_f)|_{r=50} = \lambda_s \frac{\partial T_s}{\partial r}|_{r=50} \quad (7)$$

where, h_{sf} is the convective heat transfer coefficient calculating according to the Dittus–Boelter formula [34].

$$h_{sf} = 0.023 \lambda_f \frac{\text{Re}^{0.8} \text{Pr}^{0.4}}{d_e} \quad (8)$$

where, the symbol d_e denotes the hydraulic diameter, $d_e = 100 \text{ m}$.

2.4. Numerical Method

The finite volume method with the implicit scheme is used to discretize these equations [35,36]. The algorithm of SIMPLE (Semi-Implicit Method for Pressure Linked Equation) is used to address the pressure-velocity coupling [35]. Additionally, Equations (3)–(6) together with the initial and boundary conditions are solved using MATLAB software [36]. The same model is used to evaluate the performance of EGS in references [30,33], and the uniform porosity and permeability for porous medium and the local thermal non-equilibrium equation are likewise considered. Therefore, the model used in this study can be validated through references [30,33].

3. Results and Discussion

In Figure 3a, only geothermal energy is used to provide heat for buildings. For the first fourteen years, the annual mean P_g ranges from 4772.73 to 4268.73 kW, with a percentage reduction of 10.56%. The annual mean P_g decreases drastically after fourteen years, indicating that the service life for stable output is 14 years in terms of reservoir behavior and operation conditions. The average P_g in the first fourteen years is 4521.1 kW, which can provide heat for $129,174.3 \text{ m}^2$ buildings with specific heat load of 35 W/m^2 and can reduce carbon dioxide emissions by 13,671.8 tons per heating season.

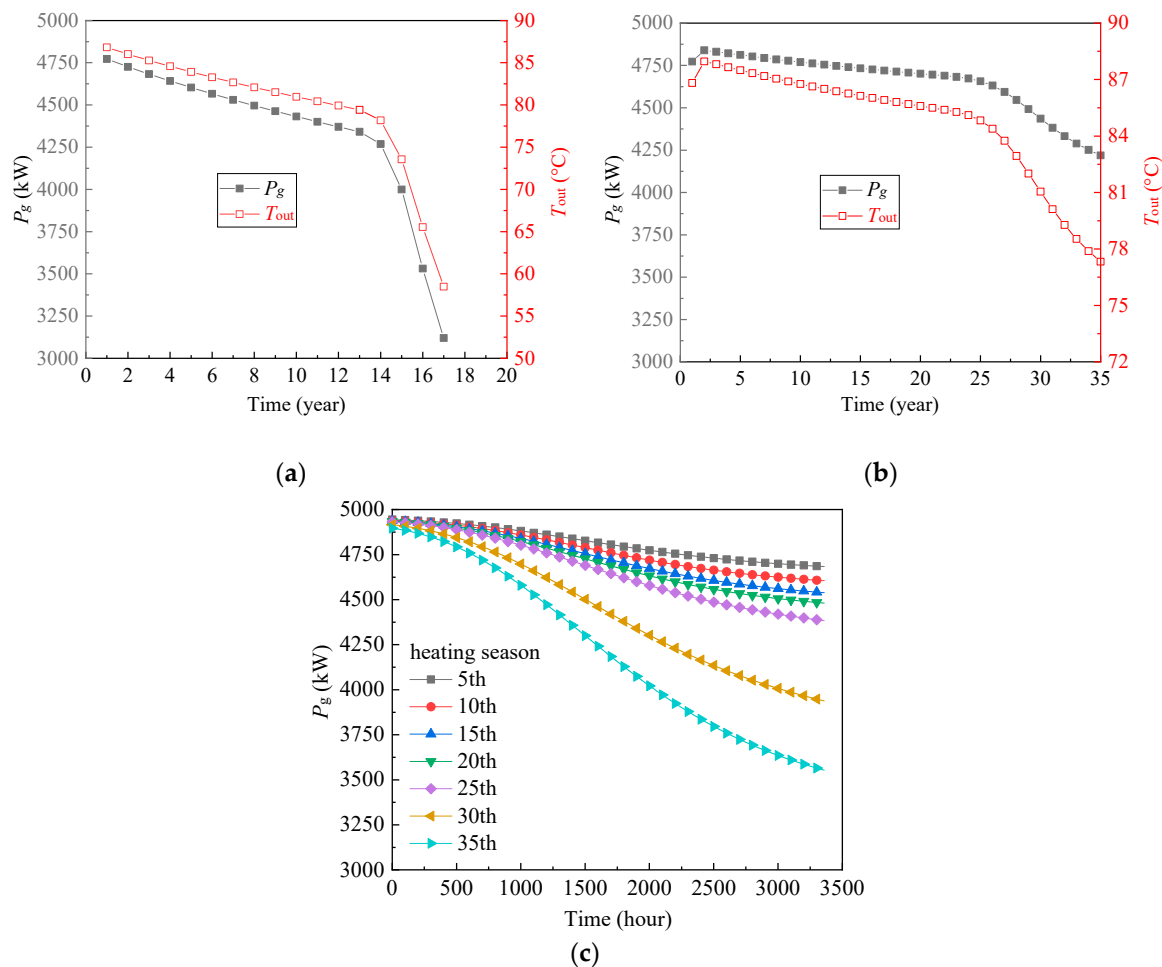


Figure 3. (a) P_g and T_{out} VS. Time for only geothermal heating without solar energy; (b) P_g and T_{out} VS. Time for hybrid geothermal and solar energy heating; (c) P_g variation from the beginning to the end at different heating seasons for hybrid geothermal and solar energy heating.

Figure 3b shows the performance of the hybrid geothermal and solar energy heating system. In the heating season, the daily mean P_s is 897.15 kW for $\eta = 0.5981$. In the non-heating season, the daily mean P_s is 1486.80 kW for $\eta = 0.6797$. It is obvious from Figure 3b that the annual mean P_g decreases gradually for the first twenty-four years, and then it decreases quickly after twenty-four years. The average P_g in the first twenty-four years is 4752.19 kW. In the first heating season, the annual mean P_g is 4772.73 kW, which is the same as that of only geothermal energy heating. From the second to twenty-fourth heating season, the annual mean P_g ranges from 4839.50 to 4672.94 kW, with percentage reduction about 0.15% per year. P_g for the first heating season is less than that for the second heating season due to having no heat from solar energy stored into geothermal reservoir in the first heating season. The average P_g of 35 years of operation is 4653.78 kW for the hybrid heating system. The P_g difference between the second and the thirty-fifth heating season is 620.63 kW, with a percentage reduction of 12.82%. The daily mean P_s is 897.15 kW, and the average P_t for 35 years of operation is 5550.93 kW, which can provide heat for 158,598.20 m² buildings with a specific heat load of 35 W/m². For the hybrid heating system, the annual mean P_g is 4218.87 kW for the thirty-fifth heating season, which is much the same as that of the fourteenth heating season for only geothermal heating systems. To sum up, the service life for a hybrid geothermal and solar energy heating system is 35 years compared to only geothermal energy heating system due to the solar energy heat stored in a geothermal reservoir.

Figure 3c shows the variation of P_g from the beginning to the end of each heating season for both geothermal and solar energy. From Figure 3c there is an attenuation for P_g from the beginning to the end of each heating season, and the attenuation degree becomes bigger with the increase in heating

years. For the fifth heating season, the attenuation degree of P_g is 5.27% from the beginning to the end of the heating season, while it is, respectively, 6.79%, 8.08%, 9.20%, 11.11%, 19.89% and 27.43% for the 10th, 15th, 20th, 25th, 30th and 35th heating seasons.

From Figure 3b,c, it can be concluded that P_g is unstable during same heating season and the different heating season at the fixed injection water temperature (5 °C) and volume flow rate (50 m³/h). Moreover, the energy supply of solar heat is unstable and discontinuous. Furthermore, the building heating loads vary with outdoor air temperature. To keep the steady running of the heating system, geothermal energy should be able to adjust the instability and meet the requirements of building thermal loads.

From the viewpoint of heat transfer principles, two main methods can be used to adjust heat transfer between rocks and fluid in term of the existing geothermal reservoir. The first method is to change the heat transfer coefficient, which can be implemented by changing the volume flow rate. The second method is to adjust the heat transfer temperature difference, which can be implemented by changing the injection water temperature.

The symbols Q and T_{in} , respectively, represent the volume flow rate and injection water temperature. From Figure 4, the annual mean P_g is 6667.81 kW at $Q = 70$ m³/h and $T_{in} = 5$ °C, and it becomes 3897.73 kW at $Q = 50$ m³/h and $T_{in} = 20$ °C. Figure 4 indicates that Q and T_{in} have an important effect on P_g . As is evident in Figure 4, a higher Q will cause a higher convective heat transfer coefficient between geothermal artificial reservoir and fluid, thus leading to a greater P_g . Generally, the pump power has almost a cubic relationship with flow velocity. As a result, an increase in Q will cause a rapidly increase in pump power. In the actual project, the pump power and P_g should thus be comprehensively considered in order to decide a reasonable Q . In addition, a decrease in T_{in} causes an increase in temperature difference between rock and fluid, thus resulting in an increase in P_g . To sum up, it can be concluded from Figure 4 that P_g can be adjusted easily by changing the injection water temperature and volume flow rate.

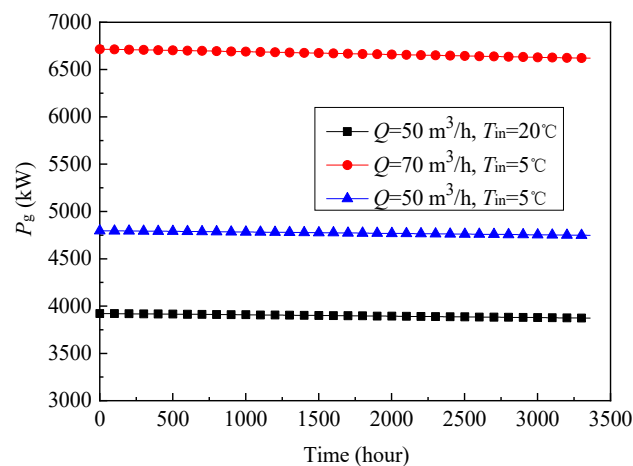


Figure 4. Variation of P_g with T_{in} and Q .

The average P_t of 5550.93 kW from geothermal (4653.78 kW) and solar energy (897.15 kW) is used as the designed heating load, and it can provide heat for 158,598.20 m² buildings with a specific heat load of 35 W/m². The coldest weather comes in January (in the middle of heating season, China), and thus the actual heating load in January is generally greater than the designed heating load. The actual heating load in the middle of heating season is assumed to be 20% greater than the designed heating load. Similarly, the actual heating load is less than the designed heating load at the beginning and end of each heating season. Furthermore, the actual heating load is assumed to be 20% less than the designed heating load at the beginning and end of each heating season. The hybrid heating system will be safe if it can meet the heating load requirement in the 35th heating season due to having minimum P_g . In the middle of the 35th heating season, the actual heating load is 6661.12 kW, and it is 4440.74 kW

at the beginning and end of heating season. From Figure 3c, at $Q = 50 \text{ m}^3/\text{h}$ and $T_{in} = 5 \text{ }^\circ\text{C}$, P_g is, respectively, 4196.54 and 3553.61 kW at the middle and at the beginning and end of the 35th heating season, therefore, the difference between the actual heating load and P_g is, respectively, 2464.58 and 887.13 kW. From Figure 4, the difference of 887.13 kW at the end of heating season is easy to adjust by changing Q and T_{in} . In the middle of heating season with the coldest weather, only geothermal energy should be able to provide heat for all buildings if solar collectors do not work. From Figure 4, at $Q = 70 \text{ m}^3/\text{h}$ and $T_{in} = 5 \text{ }^\circ\text{C}$, the annual mean of P_g is 6667.81 kW, which is greater than the maximum value of actual heating load of 6661.12 kW, indicating that the design for the hybrid geothermal and solar energy heating system is reasonable. That is to say, the maximum heat loads requirement can be met by adjusting injection water temperature and volume flow rate even though solar collectors do not work.

The performance of DBHE in winter mode, without and with solar heat storage, is shown in Figure 5. The area of solar collectors is 270 m^2 in Figure 5. DBHE is a closed loop system and circulating fluid is not directly in contact with surrounding rocks, avoiding the problem of corrosion, scale formation and fluid losses occurring frequently in the open-loop system. However, in the closed loop system of DBHE, the heat conduction through rocks is the main heat transfer pattern, limiting its performance improvement due to the poor thermal conductivity of rocks. Likewise, storing heat from solar energy into DBHE is also restricted due to rock having poor thermal conductivity. We calculate several different solar collector areas and conclude that solar collectors with an area of 270 m^2 is appropriate and matched to DBHE with depth of 2600 m (the other parameters are the same as that of SDEGS, as described in Section 2.1). While for SDEGS, the heat convection is formed in the artificial reservoir, whose heat transfer coefficient is far greater than that of heat conduction. For SDEGS, solar energy is able to store in geothermal reservoirs during the non-heating season, while during the heating season heat energy is also able to be extracted from geothermal reservoirs. Thus, a larger area of solar collectors ($10,000 \text{ m}^2$) is needed for SDEGS.

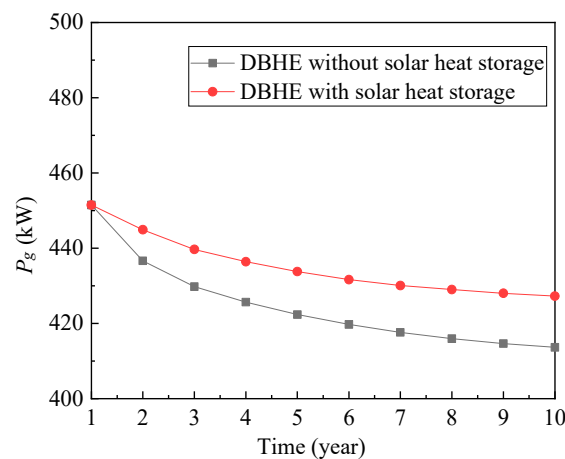


Figure 5. Performance of DBHE without any artificial reservoir.

4. Conclusions

Although China has rich heat energy reserves in hot dry rock, the technology used to exploit this at the present stage is immature. In addition, hydrothermal geothermal resources in China are also rich, however, the developed resources are far below the potential estimates due to scattered resources and low output of a single well. To efficiently utilize a low output geothermal well, a shallow depth enhanced geothermal system (SDEGS) is proposed, which can be implemented by hydraulic fracturing technology to transform the shallow depth hydrothermal system into an EGS. The shallow depth hydrothermal system has natural fractures, and it is easy to conduct hydraulic fracturing to create new fractures and highly conductive zones, and thus leading to the reduction of the hydraulic fracturing risk.

Only SDEGS with an artificial reservoir volume of $3.93 \times 10^6 \text{ m}^3$ provides heat for buildings, the service life for almost stable output is 14 years with the average P_g of 4521.10 kW. To extend the service life of geothermal reservoir, the hybrid SDEGS and solar energy heating system is proposed, which installs 10,000 m^2 solar collectors by the roof-integrated technology to store heat in geothermal reservoirs. For the hybrid heating system, the average P_g for the 35 years of operation is 4653.78 kW at $Q = 50 \text{ m}^3/\text{h}$ and $T_{in} = 5^\circ\text{C}$, and it can provide heat for building areas of 158,598.20 m^2 plus solar energy. In the middle of heating season with the coldest weather, the maximum value of actual heating load with building areas of 158,598.20 m^2 is 6661.12 kW, only geothermal energy can provide heat output of 6667.81 kW at $Q = 70 \text{ m}^3/\text{h}$ and $T_{in} = 5^\circ\text{C}$ even if solar collectors do not work. The hybrid SDEGS and solar energy heating system can extend the service life of SDEGS by storing solar energy heat in geothermal reservoirs and solve the problem of unstable and discontinuous energy supply for solar energy, as well as adjust the geothermal thermal output easily to meet the requirements of building thermal loads varying with outdoor air temperature. As a result, the smog problem in China caused by winter heating using fossil energy can be effectively solved by applied SDEGS technology and the hybrid SDEGS and solar energy heating technology due to having many shallow depth hydrothermal systems in China.

Compared with DBHE, the cost is one of the main factors obstructing the installation of SDEGS. Therefore, the effect of cost on SDEGS should be considered in future studies.

Author Contributions: Conceptualization, Y.H.; writing—original draft preparation, X.B. All authors have read and agreed to the published version of the manuscript.

Funding: This work was supported by the National Natural Science Foundation of China (No. 41972314).

Acknowledgments: We thank D. D. Zhang, H. S. Li, L. B. Wang, Y. L. Gong, and W. B. Ma for contributions to this work.

Conflicts of Interest: The authors declare no conflict of interest.

References

1. Hou, J.; Cao, M.; Liu, P. Development and utilization of geothermal energy in China: Current practices and future strategies. *Renew. Energy* **2018**, *125*, 401–412. [[CrossRef](#)]
2. Moya, D.; Aldásd, C.; Kaparajue, P. Geothermal energy: Power plant technology and direct heat applications. *Renew. Sustain. Energy Rev.* **2018**, *94*, 889–901. [[CrossRef](#)]
3. Su, C.; Madani, H.; Palm, B. Heating solutions for residential buildings in China: Current status and future outlook. *Energy Convers. Manag.* **2018**, *177*, 493–510. [[CrossRef](#)]
4. Vanderzwaan, B.; Longaa, F.D. Integrated assessment projections for global geothermal energy use. *Geothermics* **2019**, *82*, 203–211. [[CrossRef](#)]
5. Rubio-Maya, C.; Ambríz Díaz, V.M.; Pastor, M.E.; Belman-Flores, J.M. Cascade utilization of low and medium enthalpy geothermal resources—A review. *Renew. Sustain. Energy Rev.* **2015**, *52*, 689–716. [[CrossRef](#)]
6. Keçebas, A. Exergoenvironmental analysis for a geothermal district heating system: An application. *Energy* **2016**, *94*, 391–400. [[CrossRef](#)]
7. Pandey, S.N.; Vikram, V.; Chaudhuri, A. Geothermal reservoir modeling in a coupled thermo-hydro-mechanical-chemical approach: A review. *Earth-Sci. Rev.* **2018**, *185*, 157–1169. [[CrossRef](#)]
8. Asaia, P.; Panja, P.; Velasco, R. Fluid flow distribution in fractures for a doublet system in Enhanced Geothermal Systems (EGS). *Geothermics* **2018**, *75*, 171–179. [[CrossRef](#)]
9. Cheng, Q.L.; Wang, X.N.; Ghassemi, A. Numerical simulation of reservoir stimulation with reference to the Newberry EGS. *Geothermics* **2019**, *77*, 327–343. [[CrossRef](#)]
10. Bagalkot, N.; Kumar, G. Thermal front propagation in variable aperture fracture–matrix system: A numerical study. *Sadhana* **2015**, *40*, 605–622. [[CrossRef](#)]
11. Olasolo, P.; Juárez, M.C.; Morales, M.P. Enhanced geothermal systems (EGS): A review. *Renew. Sustain. Energy Rev.* **2016**, *56*, 133–144. [[CrossRef](#)]

12. Bagalkot, N.; Zare, A.; Kumar, G. Influence of fracture heterogeneity using linear congruential generator (lcg) on the thermal front propagation in a single geothermal fracture-rock matrix system. *Energies* **2018**, *11*, 916. [\[CrossRef\]](#)
13. McClure, M.W.; Horne, R.N. An investigation of stimulation mechanisms in Enhanced Geothermal Systems. *Int. J. Rock Mech. Min. Sci.* **2014**, *72*, 242–260. [\[CrossRef\]](#)
14. Zhang, W.; Qu, Z.Q.; Guo, T.K. Study of the enhanced geothermal system (EGS) heat mining from variably fractured hot dry rock under thermal stress. *Renew. Energy* **2019**, *143*, 855–871. [\[CrossRef\]](#)
15. Alimonti, C.; Soldo, E. Study of geothermal power generation from a very deep oil well with a wellbore heat exchanger. *Renew. Energy* **2016**, *86*, 292–301. [\[CrossRef\]](#)
16. Gharibi, S.; Mortezaazadeh, E.; Bodi, S.J.H.A.; Vatani, A. Feasibility study of geothermal heat extraction from abandoned oil wells using a U-tube heat exchanger. *Energy* **2018**, *153*, 554–567. [\[CrossRef\]](#)
17. Cheng, W.L.; Liu, J.; Nian, Y.L. Enhancing geothermal power generation from abandoned oil wells with thermal reservoirs. *Energy* **2016**, *109*, 537–545. [\[CrossRef\]](#)
18. Noorollahi, Y.; Pourarshad, M.; Jalilinasrabady, S.; Yousefi, H. Numerical simulation of power production from abandoned oil wells in Ahwaz oil field in southern Iran. *Geothermics* **2015**, *55*, 16–23. [\[CrossRef\]](#)
19. Fang, L.; Diao, N.R.; Shao, Z.K. A computationally efficient numerical model for heat transfer simulation of deep borehole heat exchangers. *Energy Build.* **2018**, *167*, 79–88. [\[CrossRef\]](#)
20. Gordon, D.; Bolisetti, T.; Ting, D.S.K.; Reitsma, S. Short-term fluid temperature variations in either a coaxial or U-tube borehole heat exchanger. *Geothermics* **2017**, *67*, 29–39. [\[CrossRef\]](#)
21. Bu, X.B.; Ran, Y.M.; Zhang, D.D. Experimental and simulation studies of geothermal single well for building heating. *Renew. Energy* **2019**, *143*, 1902–1909. [\[CrossRef\]](#)
22. Bu, X.B.; Jiang, K.Q.; Li, H.S. Performance of geothermal single well for intermittent heating. *Energy* **2019**, *186*, 115858. [\[CrossRef\]](#)
23. Li, H.S.; Ma, W.B.; Lian, Y.Y.; Wang, X.L. Estimating daily global solar radiation by day of year in China. *Appl. Energy* **2010**, *87*, 3011–3017. [\[CrossRef\]](#)
24. Ge, T.S.; Wang, R.Z.; Xu, Z.Y.; Pan, Q.W.; Du, S.; Chen, X.M.; Ma, T.; Wu, X.N.; Sun, X.L.; Chen, J.F.; et al. Solar heating and cooling: Present and future developmeng. *Renew. Energy* **2018**, *126*, 1126–1140. [\[CrossRef\]](#)
25. Li, P.C.; Li, J.; Pei, G.; Munir, A.; Ji, J. A cascade organic Rankine cycle power generation system using hybrid solar energy and liquefied natural gas. *Sol. Energy* **2016**, *127*, 136–146. [\[CrossRef\]](#)
26. Wight, N.M.; Bennett, N.S. Geothermal energy from abandoned oil and gas wells using water in combination with a closed wellbore. *Appl. Eng.* **2015**, *89*, 908–915. [\[CrossRef\]](#)
27. Caulk, R.A.; Tomac, I. Reuse of abandoned oil and gas wells for geothermal energy production. *Renew. Energy* **2017**, *112*, 388–397. [\[CrossRef\]](#)
28. Nian, Y.L.; Cheng, W.L. Insights into geothermal utilization of abandoned oil and gas wells. *Renew. Sust. Energy Rev.* **2018**, *87*, 44–60. [\[CrossRef\]](#)
29. Song, X.Z.; Wang, G.S.; Shi, Y. Numerical analysis of heat extraction performance of a deep coaxial borehole heat exchanger geothermal system. *Energy* **2018**, *164*, 1298–1310. [\[CrossRef\]](#)
30. Cao, W.J.; Huang, W.B.; Jiang, F.M. A novel thermal-hydraulic-mechanical model for the enhanced geothermal system heat extraction. *Int. J. Heat Mass Transf.* **2016**, *100*, 661–671. [\[CrossRef\]](#)
31. Huang, W.B.; Cao, W.J.; Jiang, F.M. A novel single-well geothermal system for hot dry rock geothermal energy exploitation. *Energy* **2018**, *162*, 630–644. [\[CrossRef\]](#)
32. Huang, W.B.; Cao, W.J.; Jiang, F.M. Heat extraction performance of EGS with heterogeneous reservoir: A numerical evaluation. *Int. J. Heat Mass Transf.* **2017**, *108*, 645–657. [\[CrossRef\]](#)
33. Jiang, F.M.; Luo, L.; Chen, J.L. A novel three-dimensional transient model for subsurface heat exchange in enhanced geothermal systems. *Int. Commun. Heat Mass Transf.* **2013**, *41*, 57–62. [\[CrossRef\]](#)
34. Zhang, X.M.; Ren, Z.P.; Mei, F.M. *Heat Transfer*, 4th ed.; China Construction Industry Press: Beijing, China, 2001.
35. Li, R.X. *Basis of Finite Volume Method*, 2nd ed.; National Defense Industry Press: Beijing, China, 2008.
36. Tao, W.Q. *Numerical Heat Transfer*, 2nd ed.; Xi'an Jiao Tong University Press: Xi'an, China, 2001.

